Water Resources Research

RESEARCH ARTICLE
10.1029/2021WR031661

Special Section:
Advancing process representation in hydrologic models: Integrating new concepts, knowledge, and data

On the Prediction of the Characteristic Times of River Meander Cutoff Sequence: Theoretical Model and Comparison With Laboratory and Field Observations

M. Pannone[1] and A. De Vincenzo[1]

[1]School of Engineering, University of Basilicata, Potenza, Italy

Key Points:

- An analytical solution in terms of dimensionless fluid-mechanical circulation versus dimensionless time is for the first time provided in the literature for the modeling of river meander cyclic growth and death and the prediction of the related characteristic times and parameters. The proposed theoretical model hinges on the potential flow approach as the limiting case of Navier-Stokes-governed fluxes at very low Reynolds numbers around fast rotating cylinders. Its main distinctive value consists in the simple closed-form solution and in the capability to account for the periodic nature of river bend cutoff
- An ad hoc-designed laboratory experiment was performed in the Laboratory of Hydraulics and Hydraulic Constructions at University of Basilicata to validate the theoretical model in terms of neck width reduction as a function of time in near-cutoff conditions (i.e., when the correct timing of the process can become a matter of safety even more than management)
- The results of the validating laboratory tests, jointly with the comparison between theoretical predictions and 20-year observations at a cutoff site on river Bollin (UK) as reported by Hooke (1995, 2004), reveal the excellent performance of the non-calibrated theoretical model in predicting times to cutoff, times from cutoff and rates of bank erosion. Thus, the model may represent a reliable, fast and easy tool to forecast the evolution of a river bend when the signs of the incipient instability suggest quantifying the time left to its exploitation as a naturalistic or an economical resource, and to timely plan suitable management and restoration interventions

Abstract River meander dynamics inevitably interferes with a number of human activities and productive processes. Therefore, investigating the involved physical processes and modeling their space-time evolution represent a crucial requirement in terms of sustainable river management and restoration planning. In the present study, a deterministic integral-differential equation that governs river-bend growth and death in the absence of natural or anthropic forcing is for the first time derived and solved by resorting to cardinal fluid-mechanical equations such as Navier-Stokes' in the Lamb-Oseen version. The related 1-D model, which accounts for morphology and sedimentology via the meander migration rate and its radius of curvature, proves to be able to grasp the periodic nature of the phenomenon. Additionally, it exhibits an overall very good agreement with field pre-cutoff and post-cutoff observations, as well as with the outcome of an ad hoc-designed laboratory experiment that simulated near-cutoff conditions. Hence, it may represent a fast and easy tool to monitor river bend hydro-geomorphological evolution, particularly when the signs of the incipient instability suggest quantifying the time left to its routine exploitation and to timely plan, where needed, suitable management and restoration interventions.

1. Introduction

Natural evolution of lowland rivers typically involves the continuous elongation of their axis, the formation of simple or compound loops, and the occurrence of cutoffs. Cutoff is the bypass of a meander loop by a shorter straight path and the consequent formation of an abandoned reach, the so-called oxbow lake. Meander cutoffs in alluvial valleys form either by the progressive narrowing of the neck until the two opposite limbs meet, or by the formation of a chute channel directly across the meander neck itself.

Lewis and Lewin (1983) reserve the term "neck cutoff" to cases in which the opposite limbs of the bend were considerably less than a channel width apart at the time of breaching, while using "chute cutoff" for cases in which a much longer breach channel was created. Since cutoff events are cyclically sporadic and are recognized to trigger important geomorphologic processes (Mosley, 1975), their occurrence practically identifies two different characteristic timescales: a short timescale, which refers to the evolution of single meanders before the cutoff, and a long timescale, which includes multiple, more or less periodic cutoffs (see also Camporeale et al., 2005; Hooke, 2004).

The study of the role of cutoff occurrence at large river dynamics timescales is usually carried out according to two different though interconnected approaches: the descriptive/experimental and the numerical method. The descriptive method dates back to very classical studies, where it was aimed at deriving some empirical laws that could relate the hydraulics of the process to the representative geomorphological parameters (e.g., Carlston, 1965; Hansen, 1967; Leopold & Wolman, 1960). From then, several laboratory/field surveys concerning cutoff (chute or neck) events, oxbow lake formation and post-cutoff adjustments have been carried out (e.g., Gay et al., 1998; Grenfell et al., 2012; Grenfell et al., 2014; Hooke, 1995; Johnson & Paynter, 1967; Li et al., 2022; Richards & Konsoer, 2019; Van Dijk et al., 2012; Van Dijk et al., 2014; Zinger et al., 2011; Zinger et al., 2013). At the same time, a number of theoretical/computational models describing meandering dynamics (e.g., Asahi et al., 2013; Eke, Czapiga, et al., 2014; Ikeda et al., 1981; Mahato et al., 2022; Seminara et al., 2001; Smith & McLean, 1984; Zolezzi & Seminara, 2001) and cutoff occurrence (e.g., Howard, 1984; Stølum, 1996; Sun et al., 1996) have been developed to simulate the planimetric evolution of rivers.

Correspondence to:
M. Pannone,
marilena.pannone@unibas.it

Citation:
Pannone, M., & De Vincenzo, A. (2022). On the prediction of the characteristic times of river meander cutoff sequence: Theoretical model and comparison with laboratory and field observations. *Water Resources Research*, *58*, e2021WR031661. https://doi.org/10.1029/2021WR031661

Received 22 NOV 2021
Accepted 28 JUN 2022

Author Contributions:
Data curation: A. De Vincenzo
Investigation: A. De Vincenzo
Validation: A. De Vincenzo

Some important aspects related to meander life cycle have emerged from a few landmark studies: the interactions between meander migration and sedimentation processes (e.g., Howard, 1984), some clues on self-organized criticality and self-confinement of the meander belt (e.g., Stølum, 1996), some evidence of the achievement of a statistically steady state for the geometrical characteristics of river planimetry (e.g., Howard, 1984; Stølum, 1996), and the recognition of the important phenomenon known as the "secondary lobe" (double heading) formation (Brice, 1974; Ferguson, 1984; Lancaster & Bras, 2002).

In a relatively recent study by Camporeale et al. (2008), the dynamical mechanisms by which cutoff events are able to influence long-term river evolution have been discussed. Particularly, the authors point out that cutoffs play two fundamental roles: (a) removing older meanders, thus limiting the geometrical complexity driven by the related fluid dynamic processes, and (b) acting as a shot noise able to influence the space-time dynamics of the whole river planimetry by the removal of the short-term spatial memory. In order to investigate the fluid-dynamic mechanisms based on which cutoffs accomplish their dissipative function, a theoretical model is proposed in the present study for the prediction of the characteristic times of meander growth and death. The model, which applies to cases in which cutoff occurs as a consequence of neck wall collapse driven by critic hydraulic gradient overcoming (therefore, in no-overbank flow conditions), produced an analytical closed-form solution. To our knowledge, it is the only fully analytical solution so far appeared in the literature for the modeling of the cyclic phases of river meander life. The inspiring background is represented by the large-scale similitude between the geometry of the near-cutoff meander axis and part of the boundary streamline of a two-dimensional uniform flow that hits a vertical-axis cylinder with increasing circulation. Note that the term boundary streamline is here referred to the potential flow streamline to which the two (or the single) cylinder stagnation points belong.

At the drainage basin scale, river bend evolution and migration that take place through rough, high resistance bed materials may indeed be thought as represented by a single streamline of an incompressible, slow sediment-flow governed by the classic Navier-Stokes equations, and perturbed by more or less space-time periodic undulations. Therefore, the relevant velocity scale for the construction of the low Reynolds number we will be referring to in the proposed analogical model is represented by the meander train downstream migration rate.

Due to its analytical nature, the model is straightforwardly applicable for a quick prediction of the time left to the routine bend exploitation (as a naturalistic or an economic resource), and the timely planning, if needed, of site management and restoration.

2. Formulation

Were a (uniform) potential fluid flow of velocity v_0'' and density ρ hitting an (eventually rotating) infinite-axis cylinder of radius r_0 in the horizontal x-y plane, the suitable dimensionless version of Navier-Stokes equations (momentum and continuity) would be (e.g., Batchelor, 1967; Marchi & Rubatta, 1981):

$$\frac{\partial \boldsymbol{v}^*}{\partial \tau} + \boldsymbol{v}^* \cdot \nabla \boldsymbol{v}^* = -\nabla p^* + \frac{1}{Re}\nabla^2 \boldsymbol{v}^* \tag{1}$$

$$\nabla \cdot \boldsymbol{v}^* = v^*_{x,x} + v^*_{y,y} = 0 \tag{2}$$

where $\boldsymbol{v}^* = \left(v_x^*, v_y^*\right)$ indicates the dimensionless local velocity vector, p^* the dimensionless local pressure, τ the dimensionless time, Re the Reynolds number and ∇ the nabla differential operator. The related scales for length, velocity, time and pressure would respectively be: $2r_0$, v_0'', $2r_0/v_0''$, and $\rho {v_0''}^2$. The numerical solution of this type of problem had allowed Padrino and Joseph (2006) to show that: (a) for a given, relatively small $Re = 2\rho v_0'' r_0/\mu$ (specifically, $Re = 200$), where μ indicates fluid dynamic viscosity, and dimensionless cylinder peripheral speed $v_c^* = v_c/v_0''$ ranging between 3 and 5, the drag coefficient $C_D = D/\rho {v_0''}^2 r_0$ (with D indicating drag) is order of 10^{-2} while the lift coefficient $C_L = L/\rho {v_0''}^2 r_0$ (with L indicating lift) is order of 10; (b) for a given, relatively small value of Re (200 or 400), the vortex tail adjacent to the cylinder contour is progressively reduced as its rotation speed increases. Thus, as demonstrated in detail in Appendix A, in the presence of a relatively fast rotating cylinder in a viscous, very slow uniform flow of velocity v_0'', the near-field streamline pattern practically coincides with that of an equivalent potential uniform flow of velocity $v_0 = f\,(v_0''; Re)$ around the same cylinder with superposed free vortex of circulation $\Gamma = 2\pi r_0 v_c$.

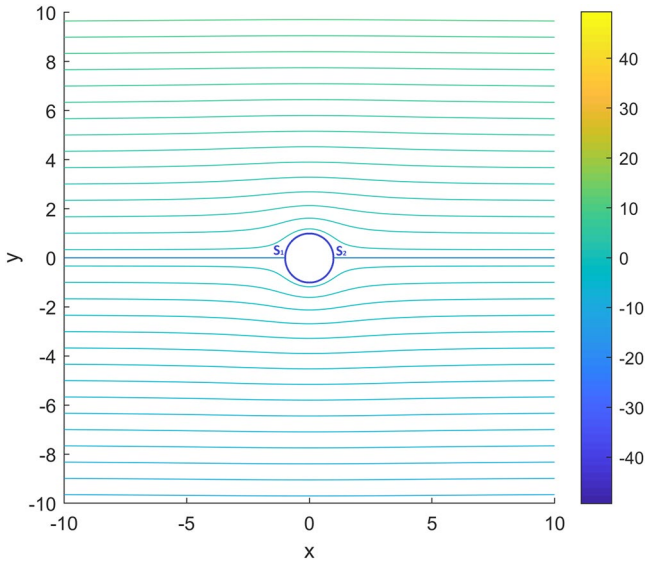

Figure 1. Potential streamline pattern of a left-to-right uniform flow of velocity v_0 that hits a cylinder of radius r_0 without circulation ($r_0 = 1$ m; $v_0 = 1$ m/s). Colorbar indicates, in m^2/s, the value of the associated stream function Ψ.

2.1. Derivation of Meander Evolution Governing Equation

It is well known that the incompressible, potential streamline that bumps against a steady cylinder of radius r_0 without circulation, within a longitudinal uniform flow of velocity v_0 in the horizontal x-y plane (Figure 1), subdivides at $S_1 = (-r_0,0)$ into two equal-length daughter streamlines (respectively characterized by clockwise/counter-clockwise direction) that reconnect downstream at $S_2 = (r_0,0)$. The axis of the river bend is represented by the clockwise daughter streamline for a bend that develops on the hydraulic left, and by the counter-clockwise daughter streamline for a bend that develops on the hydraulic right. From the potential flow theory we also know that, whereas the areas located in the neighborhood of the stagnation points experience a compression, elsewhere the cylinder is subject to traction forces. The onset of a clockwise circulation would displace the stagnation points on the hydraulic right, with the daughter streamlines that wouldn't be equal-length anymore (see Figure 2 and Figure 3 for $\Gamma/v_0r_0 = 2\pi$ and $\Gamma/v_0r_0 = 6\pi$, respectively). Note that, for $\Gamma/v_0r_0 \geq 4\pi$, there would be only one stagnation point (S) at $x = 0$ and $y < 0$. The onset of a counter-clockwise circulation would obviously produce the opposite effect. It can be useful to emphasize, at this point of the discussion, the strict similitude between the red boundary streamline in Figure 3 and the shape of the single near-cutoff loop resulting from the first approximation of Seminara et al. (2001) theoretical model as shown in their Figure 4. As a matter of fact, the periodic sequence in Seminara et al. (2001)'s Figure 4 corresponds to a final equilibrium condition characterized by zero meander amplitude time-derivative. Nevertheless, the authors themselves recognize that such a condition would hardly be achieved and that, at a certain moment before, a cutoff must occur. Accordingly, and as later discussed, the theoretical model proposed by the present study identifies the meander cutoff with the condition $\Gamma = 4\pi v_0 r_0$, associating any larger circulation like that in our Figure 3 to post-cutoff/oxbow lake formation stages. For the sake of further illustration and clarity, Figure 4 (present study) graphycally describes the geometrical analogy underlying the proposed theoretical model.

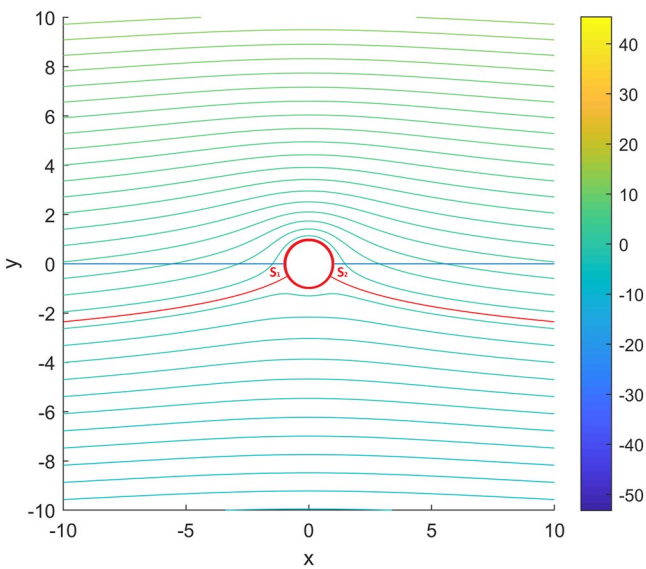

Figure 2. Potential streamline pattern of a left-to-right uniform flow of velocity v_0 that hits a cylinder of radius r_0 with circulation $\Gamma = 2\pi r_0 v_0$ ($r_0 = 1$ m; $v_0 = 1$ m/s). Colorbar indicates, in m^2/s, the value of the associated stream function Ψ.

Were the cylinder free to move, it would be forced to translate leftwards due to the positive lift increment in the case of clockwise circulation, and rightwards due to the negative lift increment in the counter-clockwise case (Magnus effect). For a fixed cylinder, the product of stagnation points displacement (the effect) and lift (the cause) gives the work done for the deformation of the boundary streamline. In the river-flow version of that basic fluid-dynamic process, stagnation-point compression is associated to the net cross-sectional accumulation of sediments in the lower velocity areas (the intrados of the bend) while traction is associated to the net cross-sectional erosion taking place in the higher velocity areas (the extrados of the bend). Additionally, cylinder pressure distribution is assimilated to a fictitious, section-averaged transverse shear stress that originates along the river from the secondary currents induced by the centrifugal/centripetal acceleration. This transverse shear stress distribution, in turn, is related to the corresponding unit-length transverse bed-load by the Meyer-Peter and Müller Equation (1948). The stream power employed to convey the bed-load, whose effect consists in deforming meander planimetry while accentuating its curvature, is equated to the power needed to displace the cylinder or, equivalently, to produce the deformation of the boundary streamline.

Let us now consider an infinite-axis cylinder undergoing low Reynolds longitudinal uniform flow, and a relatively fast clockwise rotation about its axis (allowing for a near-field potential flow approach) at rate $\Gamma/2\pi r_0^2$. As above mentioned, were the cylinder free to move, it would undergo a spin effect

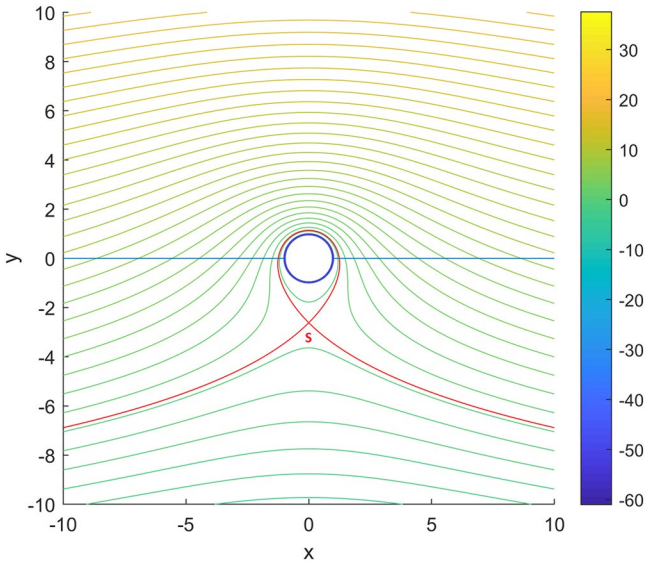

Figure 3. Potential streamline pattern of a left-to-right uniform flow of velocity v_0 that hits a cylinder of radius r_0 with circulation $\Gamma = 6\pi r_0 v_0$ ($r_0 = 1$ m; $v_0 = 1$ m/s). Colorbar indicates, in m^2/s, the value of the associated stream function Ψ.

with no boundary streamline deformation and stagnation points migration, which would indeed be compensated by cylinder transverse displacement. Were the cylinder fixed, its rotation would induce boundary streamline deformation and stagnation points transverse migration. For $\Gamma \leq 4\pi v_0 r_0$, the infinitesimal displacement of the symmetrical (in the limit coinciding) stagnation points would be (e.g., Marchi & Rubatta, 1981):

$$dy_S = \frac{d\Gamma}{4\pi v_0} \tag{3}$$

where v_0, besides the speed of the flow hitting the cylinder, can alternatively represent (with opposite sign) the speed at which the cylinder itself moves through the static fluid along the longitudinal direction. In the present analog, it must actually be viewed as the meander migration rate. The infinitesimal work done by the lift $L = \rho v_0 \Gamma$ and the related power would therefore be, respectively:

$$dW = L dy_s = \rho v_0 \Gamma \frac{d\Gamma}{4\pi v_0} \tag{4}$$

and

$$P = \frac{dW}{dt} = \frac{\rho\Gamma}{4\pi}\frac{d\Gamma}{dt} \tag{5}$$

Based on Bagnold's original stream power theory (Bagnold, 1966), the power employed by the flow to convey the infinitesimal bed-load transverse rate $dQ_b = q_b r_0 d\theta$, with q_b here indicating unit bend-length bed-load rate, is:

$$dP_b = (\gamma_s - \gamma)\, q_b \tan\alpha\, r_0 d\theta \tag{6}$$

where γ_s is the specific weight of sediment, tanα indicates sediment internal friction and θ the angular coordinate. For coarse sand or gravel bed, we will assume tan α = 0.7 (https://sites.psu.edu/tzhu/files/2016/10/Some-Useful-Numbers-1g1rkuu.pdf, 15 June 2022). Based on the Meyer-Peter and Müller formula in the Einstein notation (Einstein, 1950), q_b is derived from:

$$\Phi = 8\left(\tau_0^* - \tau_{0cr}^*\right)^{3/2} \tag{7}$$

where:

$$\Phi = \frac{q_b}{\sqrt{\frac{\rho_s - \rho}{\rho} g d_s^3}} \tag{8}$$

$$\tau_0^* = \frac{\tau_0}{(\gamma_s - \gamma) d_s} \tag{9}$$

$$\rho_s = \frac{\gamma_s}{g} \tag{10}$$

τ_0 indicates the dimensional shear stress; d_s the representative grain size; subscript *cr* critical (incipient motion) conditions, and the asterisk dimensionless quantities. As above mentioned, in the present analogical model τ_0 is assimilated to the pressure on the cylinder that exceeds the static isotropic counterpart p_0 (e.g., Marchi & Rubatta, 1981):

$$\tau_0 = p_{cil} - p_0 = \frac{\rho v_0^2}{2}\left[1 - 4\left(\sin\theta + \frac{\Gamma}{4\pi r_0 v_0}\right)^2\right] \tag{11}$$

while τ_{0cr} is given by the pressure corresponding to the ideal stable case of no circulation:

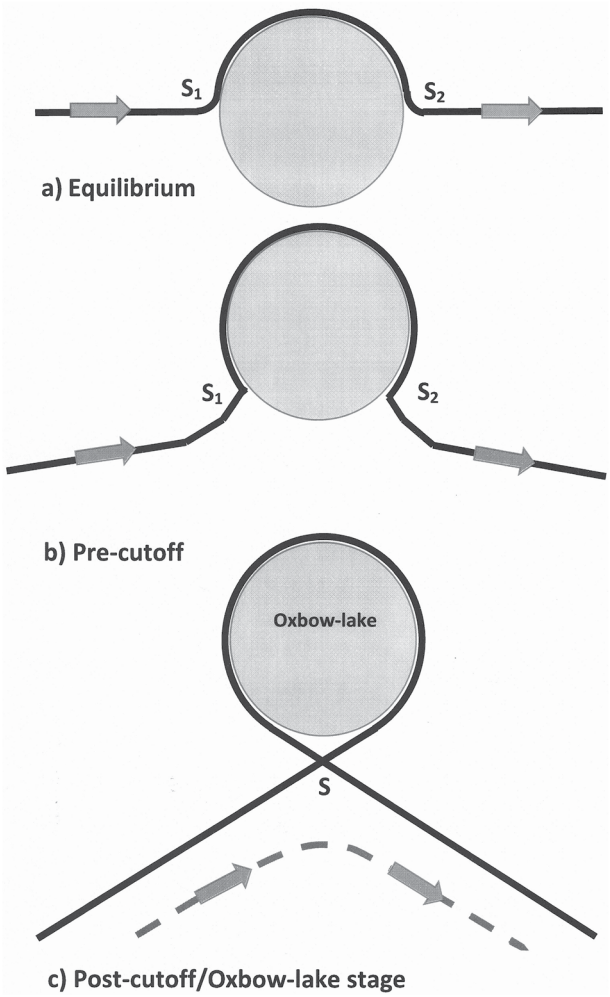

Figure 4. Illustration of the geometrical analogy underlying the proposed theoretical model; the arrows indicate river flow direction. At equilibrium and in pre-cutoff conditions, full black line indicates river axis; in post-cutoff conditions, dashed gray line indicates the post-loop closure shorter path.

$$\tau_{0cr} = \frac{\rho v_0^2}{2}\left(1 - 4\sin^2\theta\right) \tag{12}$$

Thus, provided that a work is done regardless of the sign of $\tau_0 - \tau_{0cr}$:

$$dP_b = \frac{\tan\alpha\rho v_0^3 \Gamma^{*3}}{2\sqrt{2}\pi^3}\left|-1 - \frac{8\pi\sin\theta}{\Gamma^*}\right|^{3/2} r_0 d\theta \tag{13}$$

where

$$\Gamma^* = \frac{\Gamma}{v_0 r_0} \tag{14}$$

and the vertical brackets indicate absolute value.

Since the total power given by $P_b = \int_{\beta_1(t)}^{\beta_2(t)} dP_b$, where

$$\beta_1(t) = -\sin^{-1}\left[\frac{\Gamma(t)}{4\pi r_0 v_0}\right] \tag{15}$$

and

$$\beta_2(t) = \pi + \sin^{-1}\left[\frac{\Gamma(t)}{4\pi r_0 v_0}\right] \tag{16}$$

indicate the angular coordinates of the two stagnation points, must be equated to P from Equation 5, we obtain:

$$\frac{d\Gamma^*}{d\tau} = \frac{2\Gamma^{*2}\tan\alpha}{\sqrt{2}\pi^2}\int_{\beta_1(\tau)}^{\beta_2(\tau)}\left|-1 - \frac{8\pi\sin\theta}{\Gamma^*}\right|^{3/2} d\theta \tag{17}$$

with $\tau = tv_0/r_0$. Finally, the integration of Equation 17 formally yields:

$$\Gamma^*(\tau) = \frac{2\tan\alpha}{\sqrt{2}\pi^2}\int_0^{\tau}\Gamma^{*2}(\tau')\int_{\beta_1(\tau')}^{\beta_2(\tau')}\left|-1 - \frac{8\pi\sin\theta}{\Gamma^*(\tau')}\right|^{3/2} d\theta d\tau' \tag{18}$$

Based on the potential flow theory, when $\Gamma = 4\pi v_0 r_0$ and, therefore $\Gamma^* = 4\pi$, the two stagnation points overlap and the loop is closed. In the river flow analog, we can say that this condition corresponds to the cutoff of the meander.

It is worth noting that the crucial role of the stream power in determining river morphodynamics peculiarities had already been investigated by the authors in previous studies (De Vincenzo et al., 2016; Pannone & De Vincenzo, 2021) referring to braided beds. Specifically, in De Vincenzo et al. (2016), it had been shown that a different relationship (linear or quadratic power law) between dimensionless unit bed load Φ and dimensionless unit stream power $\Omega = \gamma Q s_e / \left(B\sqrt{g(\rho_s - \rho)d_s^3/\rho}\right)$, with s_e indicating the energy slope, Q the flow rate and B the total bed width, is the expression of different morphological regimes. For values of Ω up to 1 (power law domain), all the available stream energy is employed to guarantee bed load transport and channel active bed modeling, with changes in cross-sectional geometry and bottom slope; conversely, for Ω larger than 1 (linear domain), part of the available of energy is employed to maintain suspension. In Pannone and De Vincenzo (2021), the combination of quadratic power law and sediment continuity yielded a variable-coefficients advection-diffusion equation that was numerically solved to show how, at dynamic equilibrium, the smaller the ratio of macro-bedforms wavelenght to total channel width, the more marked the tendency of the river to preserve the multi-thread flow configuration.

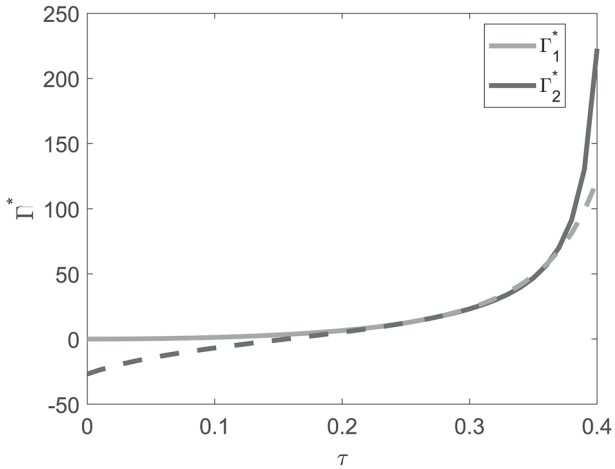

Figure 5. Matching of the asymptotic solutions for the dimensionless circulation. Γ_1^* and Γ_2^* respectively indicate short-time (Equation B6 Appendix B) and large-time curve (Equation B12 Appendix B). Length scale: r_0; velocity scale: v_0.

In order to obtain an analytical solution for the dimensionless circulation (18) that allows (a) bypassing the numerical artifacts unavoidably arising at very small and very large values of Γ^* and (b) connecting the phenomenon to known closed-form mathematical expressions, Equation 17 will first be integrated in an approximate fashion for the two limiting conditions ($\Gamma^* \to 0$ and, formally, $\Gamma^* \to \infty$ with Equations 17 and 18 reformulated accordingly from a suitable version of Equations 3 and 4). Then, a full-range solution will be found by imposing the matching of their respective extrapolations at the critical value $\Gamma^* = 4\pi$. The details of the derivation can be found in Appendix B. Note that the proposed mathematical model considers a single meander only. Therefore, it is supposed to better interpret reality when the spatial frequency of the river bends is relatively low.

2.2. Results

The solution found in Appendix B (Equations B6 and B12) is shown in Figures 5 and 6 and in Figure 8 (which encompasses periodicity and, therefore, also negative circulation values), with the horizontal line in Figure 6 that indicates the cutoff threshold. Based on the potential flow theory, neck length can then be estimated from the following trigonometric relationship (see Figure 7):

$$l_n(\tau) = 2\cos\left\{\sin^{-1}\left[\frac{\Gamma^*(\tau)}{4\pi}\right]\right\} \tag{19}$$

with $l_n = L_n/r_0$, which practically identifies, in dimensionless terms, the length of the chord between the two symmetrical stagnation points. Equations B6 and B12 in Appendix B represent periodic functions (tangent square and tangent, respectively). Once Γ^* has reached its (first) cutoff-value 4π at $\tau = 0.25079$, and after the discontinuity taking place around $\Gamma^* \to \pm\infty$ (which is physically associable with the by-pass of the bend through a straight path, and the isolation of the closed loop representing the oxbow lake), the circulation abruptly changes its sign. A new bend then starts to form on the same side (or the opposite, if the real-life geomorphological/anthropic forcing makes the evolutional process represented by a counter-clockwise circulation), reaches the zero-value that characterizes the equilibrium half-circle bend, and then increases again toward a new cut-off (Figure 8).

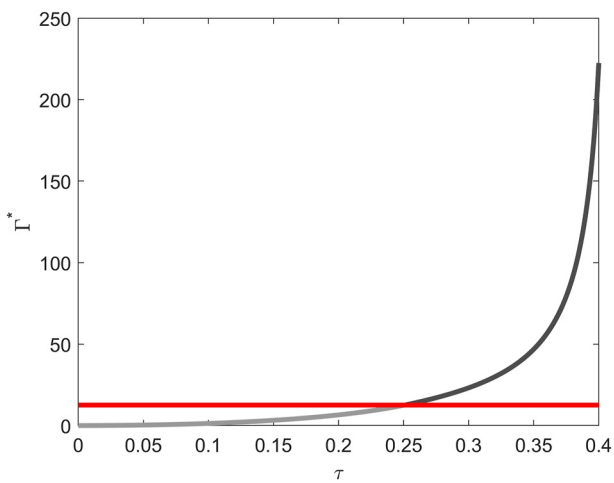

Figure 6. Equilibrium to cutoff dimensionless circulation. Horizontal line indicates cutoff threshold. Length scale: r_0; velocity scale: v_0.

3. Laboratory Experiment and Theory Validation

In order to test theory performance for dimensionless circulation values tending to the critical 4π, two different experiments were carried out according to the classical Froude similitude (Peakall et al., 1996) on an ad-hoc designed physical model that simulated the evolutional process of a typical freely meandering stream under local incipient neck cutoff conditions. The sandy alluvial floodplain (d_{50} = 0.45 mm, d_{10} = 0.1 mm, d_{90} = 2 mm, γ_s = 2,650 kg/m^3) was reproduced within a 6 m long, 5 m wide and 0.15 m deep wooden basin in the Laboratory of Hydraulics and Hydraulic Constructions at University of Basilicata (Italy). Basin bottom and side walls were made water-resistant by a silicone layer and a plastic sheet revetment; the bottom was further protected and reinforced by geotextile (Figure 9). In each experimental run, an initial meandering planform with a train of semicircular meanders, which were free to model cross-sectional geometry and bed topography in the absence of external constraints, was imposed to investigate the short timescale characterizing river evolution before the cutoff of a single meander (Camporeale et al., 2005; Frascati & Lanzoni, 2009). For that purpose, only one of the bends, far enough from floodplain inlet and outlet, reproduced high curvature, near-cutoff conditions (Figure 10). The

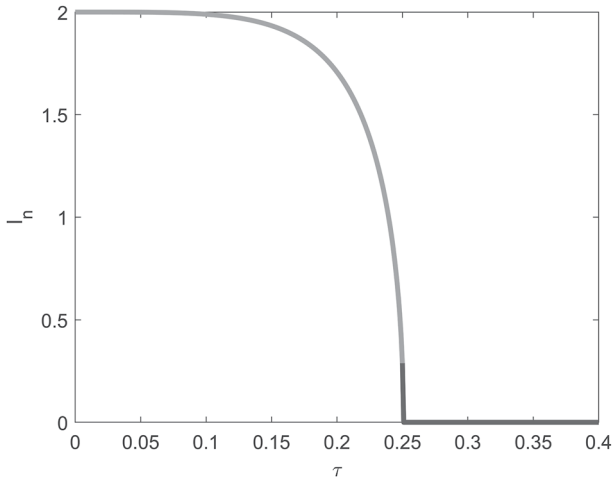

Figure 7. Equilibrium to cutoff dimensionless neck length (Equation 19). Length scale: r_0; velocity scale: v_0.

initial channel was characterized by average bottom slope $s_b = 0.008$ and rectangular cross-sections of width $B = 0.1$ m and depth $h = 0.08$ m. Clear water coming from the laboratory pipe (the model was not a recirculating system) entered the upstream inlet of the channel by a rectangular-shaped 0.07 m wide by 0.05 m high conduit, with approximately uniform streamline distribution. Flow rate Q was measured by an electro-magnetic device located on the laboratory pipe upstream of the physical model. According to model hypotheses, and provided that overbank flows are not required for neck cutoff (Gay et al., 1998; Hooke, 1995), the two runs were carried out at constant $Q = 0.00025$ m^3/s, which was a flow rate value smaller than the bankfull limit. The two runs differed in terms of critical meander centerline curvature radius r_0 and, therefore, in terms of r_0/B ratio, which is widely recognized as a morphological factor crucially affecting lateral migration rate (Hickin & Nanson, 1984; Richard et al., 2005) and meander cutting (Crosato, 2009; Yilmaz, 2008).

The initial intra-meander neck width L_n, that is, the initial distance between the two converging limbs of the critical bend, was set at 0.1 m in both runs, while r_0 was set at 0.45 m in the first run and at 0.34 m in the second (with $L_n(0)/r_{0\mathrm{I}} = l_{n\mathrm{I}}(0) = 0.222$ and $L_n(0)/r_{0\mathrm{II}} = l_{n\mathrm{II}}(0) = 0.294$, respectively).

The initial values of Shields' parameter:

$$\tau_0^*(d_{50}) = \frac{R_H s_b}{\left(\frac{\gamma_s - \gamma}{\gamma}\right) d_{50}} \tag{20}$$

with R_H indicating flow hydraulic radius, were higher than the corresponding critical threshold $\tau_{0cr}^* = 0.047$ in order to allow for in-channel sediment transport and meander morphological evolution; medium grain size d_{50}, average flow depth h and section width B placed the channel within the meandering dune regime (Yalin, 1992). Moreover, the shape parameter E as proposed by Parker (1976):

$$E = \frac{B s_e}{\pi h Fr} \tag{21}$$

where Fr indicates the flow Froude number:

$$Fr = \frac{U}{\sqrt{g R_H}} \tag{22}$$

and U the section-averaged velocity, was smaller than 1 and, therefore, typical of slow meandering rivers. The experimental surveys, which were performed on average every 4 hr before the cutoff and only once immediately after it, consisted in: (a) acquisition of water surface elevation and bed topography above a datum at 8 cross-sections along the channel, three of which were located at the apices of a few bends of the upstream train and the remaining five along the critical meander (Figure 10), by using a manual point gauge mounted on a carriage (cross-sectional measurements were spaced two cm apart); (b) acquisition of concave bank position relative to one of the floodplain model side barriers at cross-sections 1, 2 and 3; (c) measurement of the neck width. The experiments were stopped 1 hr after the neck breaching. Total experimental running times were $T_{\mathrm{I}} = 32.7$ hr and $T_{\mathrm{II}} = 30$ hr, respectively. See Table 1 for a summary of the relevant experimental parameters in incipient cutoff conditions. Sinuosity σ is referred to the closing loop (in parenthesis the average values referred to the whole train of meanders). The corresponding bend inlet deflection angle ϑ was calculated from the curve $1/\sigma = f(\vartheta)$ as reported by Yalin (1992). Finally, $Re^* = v^* d_{50}/\nu$ indicates grain Reynolds number and $v^* = \sqrt{g R_H s_e}$ shear velocity.

As an example, Figure 11 shows a picture of Run1 meander in immediate pre-cutoff and Figure 12 the details of the neck. As one can see, meander late evolution was associated to alternate bar formation with superposed dunes and water surface rippling. Capturing the position of the concave bank at cross-sections 1, 2 and 3, with the

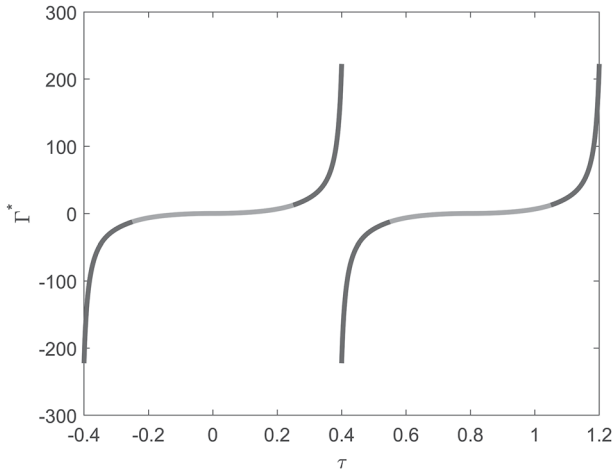

Figure 8. Double-cycle dimensionless circulation. Vertical asymptotes identify loop bypass discontinuity. Length scale: r_0; velocity scale: v_0.

cross-sectional wetted area that remained approximately constant over time, allowed us to estimate bend lateral shift and, therefore, the experimental average bank erosion rate: $v_E = 3.5 \cdot 10^{-7}$ m/s. In both experimental runs, the rate of bank erosion was also calculated according to Ikeda et al. (1981) criterion:

$$v_E = E' u'_b \tag{23}$$

which assumes a linear relationship between bank erosion rate and a function of the cross-sectionally averaged velocity (u'_b) that reflects the magnitude of concave bank shear stress. In Equation 23, E' is a coefficient of bank erosion that globally accounts for grain size, geotechnical properties of bank material, effects of the vegetation on near-bank flow, local channel slope and width, meander sinuosity, bend curvature, stream power and r_0/B ratio (Hasegawa, 1989; Ikeda et al., 1981; Odgaard, 1987; Richard et al., 2005; Wallick et al., 2006). According to Odgaard's bank erosion model (Odgaard, 1984), $v_E/E' = u'_b$ may be expressed by the following relationship:

$$\frac{v_E}{E'} = U \left\{ \left[1 + \frac{B}{2r_{out}} (k-1) \right]^{1/2} - 1 \right\} \tag{24}$$

where r_{out} is the outer bank curvature radius, k is defined by the following expression:

$$k = \frac{h_{out}}{h_0 \left(\frac{r_{out}}{r_0} - 1 \right)} \tag{25}$$

h_{out} indicates flow depth at the outer bank and h_0 flow depth at channel centerline.

Odgaard's bank erosion model was applied to cross-sections 1, 2 and 3, where the linear relationship between v_E and U can realistically be assumed to be valid. For instance, for Run2 and cross-section 3, where the wetted area A was equal to 0.0027 m^2 and the cross-sectionally averaged velocity $U = Q/A$ to 0.09 m/s, the measured values of h_{out}, r_{out}, h_0 and r_0 led to $v_E/E' = 0.078$ m/s. Assuming an erosion parameter of $5 \cdot 10^{-7}$, which is typical of sand beds (e.g., Costantine et al., 2010), an instantaneous average bank erosion rate of $3.9 \cdot 10^{-7}$ m/s was obtained, which corresponds to a daily average value of 0.033 m. As one can see, the calculated instantaneous average value of v_E was very close to that directly estimated from bend lateral shift.

Figure 9. Empty wooden basin utilized to simulate the sandy alluvial floodplain in the Laboratory of Hydraulics and Hydraulic Constructions at University of Basilicata.

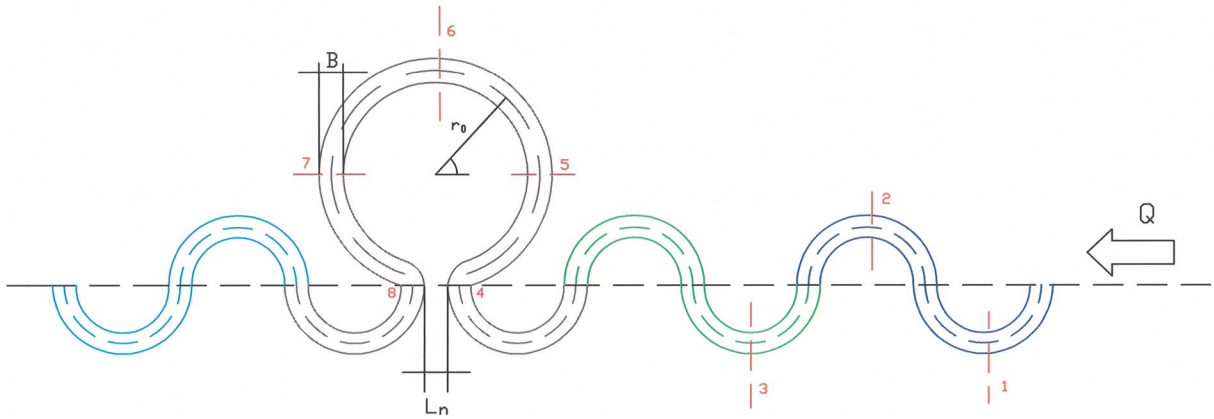

Figure 10. Scheme of the initial channel planform with the monitored cross-sections (identified by the read dashed lines and numbers). Only the meanders that proved to be completely free from boundary effects are reproduced. Dimensions are to scale (for Run2); the different colors highlight the wavelengths included in the periodic sequence, with the purple indicating the critical loop (By Mr. Antonio Cosa, MS CE).

The validation of the theory in pre-cutoff conditions (i.e., when the right timing of the process is a matter of safety more than management, and the evolutional process rapidly goes toward an abrupt discontinuity), was performed by first estimating the meander residual migration rate. From Equation 19, with $l_n = L_n/r_0$, we got the values of the theoretical dimensionless circulations at run starting ($\Gamma_I^* = 12.4887$ and $\Gamma_{II}^* = 12.4297$). Then, from Equation B12 in Appendix B:

$$\Gamma^* = \sqrt{12\pi^3}\tan(\sqrt{24\pi}\tan\alpha\tau - 0.9469)$$

we calculated the corresponding dimensionless times: $\tau_I = 0.25032$ and $\tau_{II} = 0.24997$. Finally, from the time derivative of Equation 19, which represents the dimensionless version of the theoretical bank erosion rate:

$$\frac{dl_n}{d\tau} = \frac{\Gamma^*}{8\pi^2}\frac{1}{\sqrt{1-\frac{\Gamma^{*2}}{16\pi^2}}}\frac{117.245}{\cos^2(6.078\tau - 0.9469)} = \frac{v_E}{v_0} \tag{26}$$

evaluated at the times of interest with $v_E = 3.9 \cdot 10^{-7}$ m/s, we respectively obtained $v_{0I} = 1.645 \cdot 10^{-9}$ m/s and $v_{0II} = 2.19 \cdot 10^{-9}$ m/s. Provided that, from both Equations B6 and B12 in Appendix B, $\Gamma^* = 4\pi$ at $\tau = 0.25079$, the theoretical corresponding times left to cutoff were $\Delta\tau_{cI} = 4.7 \cdot 10^{-4}$ and $\Delta\tau_{cII} = 8.2 \cdot 10^{-4}$ or, in dimensional terms, $\Delta t_{cI} = \Delta\tau_{cI} r_{0I}/v_{0I} \cong 35.7$ hr (against the experimental 32.7 hr, with +9% relative error) and $\Delta t_{cII} = \Delta\tau_{cII} r_{0II}/v_{0II} \cong 35.4$ hr (against the experimental 30 hr, with +18% relative error). See Figure 13 and Figure 14, respectively displaying dimensionless neck width versus dimensionless time in Run1 and Run2. Full black lines represent the theoretical solution; dashed black lines the corresponding 90% confidence interval; empty gray circles the experimental observations. As one can see, the (non-calibrated) analytical solution was overall able to convincingly represent the near-cutoff neck reduction process. Only the very final values of l_n fell outside the 90% confidence interval. As a matter of fact, whereas the mathematical model can follow the process until the achievement of the theoretical $l_n = 0$, in the reality, when $l_n \to 0$, the hydrostatic gradient across the neck becomes so large that the thin sandy neck wall suddenly collapses (e.g., Han & Endreny, 2014) without effectively ever reaching the theoretical zero-width condition. Thus, the experimental points of zero l_n-coordinate in Figures 13 and Figure 14 are actually representative of the immediate post-collapse condition (the only that could experimentally be detected). In any case, as above discussed, the order of magnitude of the breaching time was grasped with a definitely acceptable (and manageable) margin of error.

Table 1
Experimental Parameters in Incipient Cutoff Conditions

	Run1	Run2
τ_0^*	0.309	0.114
σ	4.08 (2.2)	3.4 (2.02)
ϑ	120°	110°
r_0/B	3.61	3.00
s_b	0.005	0.005
Fr	0.260	0.157
Re^*	200.03	121.49

Figure 11. Run1: Meander in incipient cutoff conditions.

4. Comparison With River Bollin Cutoff Site Observations (Hooke, 1995, 2004)

In order to test the theory over a wider time horizon, farer-from-cutoff conditions and, mostly, in real-life scenarios, we compared analytical solution and field observations at a cutoff site on river Bollin (Hooke (1995, 2004)). Tables 2–4 summarize the results of the validation test. River Bollin, which can be defined as an active meandering, gravel-bed river, flows in north-western England at the south of Manchester conurbation. By early November 1980, at the cutoff site, located just downstream of Mill Lane bridge near the town of Wilmslow (Cheshire), erosion had been rapidly progressing in the adjacent apices of the (double-head) loop and the banks, made of sandy alluvium, were undergoing considerable seepage. At that time, the neck of the meander had narrowed to only 1.5 m wide. Since it was clear that a neck cutoff was about to occur, the whole reach was mapped by accurate land survey on November, 8. The breach of the neck took finally place on November, 15. In immediate pre-cutoff conditions, the reported total length of the bend was equal to 232 m (radius of the equivalent circle: $r_0 = 36.92$ m). From Equations B12 and 19, the theoretical dimensionless time needed for the dimensionless neck length l_n to decrease from 1.5/36.92 = 0.0406 to 0 is $\Delta\tau_c = 2 \cdot 10^{-5}$. In order to match the real time left to cutoff on November, 8 (7 days), meander migration rate v_0 should have been equal to about $1.2 \cdot 10^{-9}$ m/s. Among other things, Hooke (1995) provides graphical details about local channel changes in time, specifically 1970, 1980 and 1989 planimetries (see Figure 15). Based on the theory proposed by the present study, at a given site, meanders are always variable-length arcs of circumference with the same constant radius. In 1970, when position, curvature and, likely, residual migration rate of the closing loop were already approximately defined and fixed (as one can see from Figures 15, 1970 and 1980 meanders are almost superposed, with the only considerable difference in terms of neck width), the graphically estimated neck length L_n was equal to about 30 m or, in dimensionless terms, $l_n = 30/36.92 = 0.81$. From Equations B12 and 19, we correspondingly obtained $\tau = 0.24418$. The dimensionless time interval needed for l_n to decrease from 0.81 to 0 therefore was $\Delta\tau_{tc} = 0.25079 - 0.24418 = 0.00661$ or, in dimensional terms, using 1980 migration rate, $\Delta t_{tc} \cong 6.5$ years, which is a value definitely close (and, for the benefit of safety, smaller) to the real time left in 1970 to cutoff (10 years). Finally, from 26:

$$\left|\frac{dl_n}{d\tau}\right|_{\tau=0.24418} = v_E/v_0|_{\tau=0.24418} \tag{27}$$

we obtained a pre-cutoff v_E of 2.16 m/year against the average pre-cutoff 1.25 detected on field (Hooke, 1995). As shown in Figure 15, in 1989 a new bend was developing on the opposite side of 1980 loop. The length of the chord between the extremes of the bend was approximately 67 m long, which gives a dimensionless neck length $l_n = 67/36.92 = 1.81$. The reported 1989 sinuosity was $\sigma = 2.49$ (Hooke, 2004). The estimated river average width was $B = 9.65$ m. Based on Ikeda's (1981) model and the corresponding curve $v_0/B = f(\sigma)$ as reported by Crosato (2009), with the migration rate given in meters per year, we found $v_0/B = 0.028$ and, therefore, $v_0 = 8.57 \cdot 10^{-9}$ m/s. For $l_n = 1.81$, Equations B12 and 19 give $\Gamma^* = 5.346$, $\tau = 0.20027$, $\Delta\tau_{fc} = 0.05052$ (dimensionless time from cut-off) and, therefore, a theoretically estimated time elapsed from cutoff of about 7 years (against the actual approximately 9). It is worth noting that Crosato's curve, which does not cover the range of sinuosity larger than 3, couldn't have been used for the pre-cutoff data set. Indeed, as also the theory predicts via the tangent function behavior, the dynamics of a meander that is approaching the cutting is a highly nonlinear and rapidly accelerating process. In the reality, neck collapse occurs suddenly, due to its narrowing beyond a critical threshold and the overcoming of the strength against the differential hydrostatic pressure. Finally, from 27

Figure 12. Run1: Details of the closing neck.

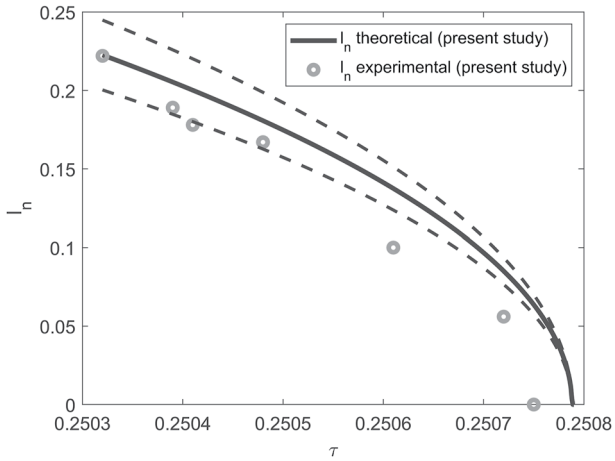

Figure 13. Neck width reduction toward cutoff in Run1: analytical solution with 90% confidence interval (dashed lines) versus experimental observations.

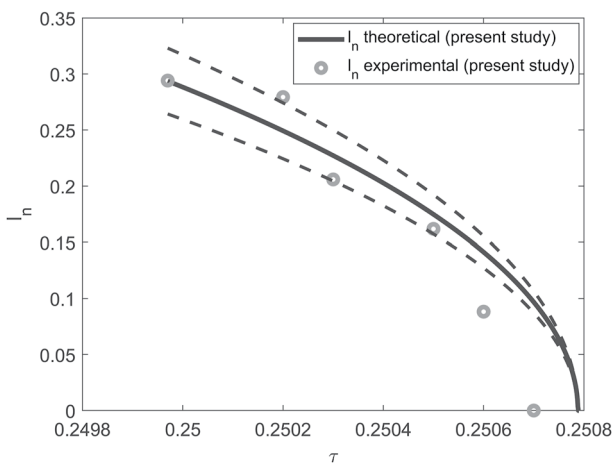

Figure 14. Neck width reduction toward cutoff in Run2: analytical solution with 90% confidence interval (dashed lines) versus experimental observations.

evaluated at $\tau = 0.20027$, we obtained a post-cutoff v_E of 2.56 m/year against the average post-cutoff 2.11 detected on field (Hooke, 1995), which, again, highlights the good predictive ability of the model.

5. Discussion and Conclusions

The present study has proposed and validated, by comparison with field and laboratory data, a theoretical model based on the potential flow theory and enabled by a suitable solution of Navier-Stokes' equations in the presence of a rapidly rotating cylinder at low Reynolds numbers. The target of the investigation is represented by the assessment of the characteristic times of river meander cyclic growth and death. The underlying motivation of the specific theoretical approach is represented by the large (basin) scale geometric similitude between the progressively more curved channel axis at cutoff site and the boundary streamline of an initially uniform flow that hits a cylinder with increasing circulation. It should be emphasized that the use of the potential flow theory (and, ultimately, Euler's equation) for the modeling of meandering river axis evolution is also legitimized, beyond the invoked geometrical analogy, by the results of Stølum's (1996) numerical simulations. These simulations, which were based on a fractal stochastic interpretation of river meanders dynamics, actually demonstrated that there exists a statistically steady-state about which the sinuosity of the whole river tends to oscillate by periodically compensating (by cutoff) its excess due to growing meanders. Indeed, one of the consequences of Euler's equation is represented by the theorem of global circulation conservation. In Stølum's simulations, this conservation is achieved (in an ensemble mean sense) by the periodic cutting of exceedingly curved and large meanders.

Recent numerical studies focusing on meander dynamics have addressed the separate dynamics of each river bank and floodplain-channel interactions. Following the novel approach by Parker et al. (2011), Eke, Parker, and Yasuyuki (2014) have modeled planform river meander evolution by introducing separate closure relations for the migration of advancing and retreating banks. Along with recent experimental work (e.g., van Dijk et al., 2014), they predict how channel width adjusts in time as a response to a dynamic "dialogue" between the two banks, by raising the question of whether width adjustments and channel migration are mostly supported by a bar push or a bank pull process. Zen et al. (2016) proposed an "at bend cross-sectional scale" model for the lateral migration of river bends, where the two banks can migrate separately as a result of the mutual interaction of river flow, sediments and riparian vegetation. The model relates the migration of the inner bank to the active role of point bar riparian vegetation dynamics by means of biophysically-based relationships for vegetation biomass growth and decay. Our study belongs to the category of "at bend axis scale" analytical models corroborated by laboratory and field validation and, to our knowledge, is the only fully analytical model of meander evolution toward cutoff existing at this time. An exhaustive review of scale issues related to general fluvial instability is reported by Dey and Ali (2020). Analytical models offer the possibility to identify (in dimensionless and, therefore, universal form) the most relevant parameters for the process under investigation. Thus, they can not only guide the design of laboratory/field/numerical tests, but also offer the *vademecum* for a timely and efficient intervention on field only where and when it is really necessary.

Process governing equation in terms of dimensionless circulation as a function of dimensionless time was obtained in the present study by making a system of the equations respectively expressing the fluid-dynamic power needed to deform the cylinder boundary streamline and the stream-power needed to convey the bed-load associated with river cross-sectional average shear-stress. The cross-sectional average shear-stress, in turn, was assumed as coinciding with the cylinder radial pressure that exceeds the value corresponding to the ideal stable case of no circulation. It must be stressed that,

Table 2
River Bollin 1980 Immediate Pre-Cutoff Observed and Estimated Variables

Immediate pre-cutoff 8 November 1980	
L_n (real) Hooke (1995)	1.5 m
r_0 (real) Hooke (1995)	36.92 m
l_n (real) Hooke (1995)	0.0406
Γ*(from Equation B3)	12.5638
τ (from Equation B2)	0.25077
$\Delta\tau_{tc}$ (theoretical)	$2 \cdot 10^{-5}$
Δt_{tc} (real) Hooke (1995)	7 days
v_0 (estimated)	**$1.2 \cdot 10^{-9}$ m/s**

Note. Bold value indicates the estimated migration rate.

Table 3
River Bollin 1970 Pre-Cutoff Observed and Calculated Variables

Pre-cutoff 1970	
L_n (real) Hooke (1995)	30 m
r_0 (expected)	36.92 m
l_n (expected)	0.81
Γ*(from Equation B3)	11.49
τ (from Equation B2)	0.24418
$\Delta\tau_{tc}$ (theoretical)	0.00661
v_0	$1.2 \cdot 10^{-9}$ m/s
Δt_{tc} (theoretical)	**6.5 years**
Δt_{tc} (real) Hooke (1995)	**10 years**
v_E/v_0 (from Equation B10 at $\tau = 0.24418$)	57.09
v_E (theoretical)	**2.16 m/year**
v_E (real) Hooke (1995)	**1.25 m/year**

Note. Bold values highlight the comparison between predictions and observations.

strictly speaking, such a formulation is fully justified only in the presence of large bend curvature in near-cutoff conditions, while representing just an approximation for the far-from cutoff regime. Such an approximation, which was in any case satisfactorily corroborated by comparison with field survey macroscopic data, is expected to be as closer to reality as slower the meander migration is. The analytical solution of the governing equation proposed in the present study (which refers to the limiting case of low Reynolds numbers and high cylinder rotation speed) is (consistently) a periodic one in the form of a tangent/tangent squared. After the cutoff, and the mathematical discontinuity represented by the $\pm\infty$ behavior (which is physically associable with the sudden breach of the neck, and the bypass of the loop by a faster straight path), a new bend (represented by $\Gamma \to -\infty$) starts to develop on the same side, gradually reaches the zero-circulation condition associated with the equilibrium half-circle shape ($\Gamma = 0$), and then continues growing toward a new cutoff ($\Gamma \to +\infty$), as graphically illustrated by the periodic solution in Figure 8. The favorable comparison of model prediction in terms of time to cutoff, time elapsed from cutoff and rates of bank erosion with the data collected from field survey at a cutoff site on river Bollin (UK), and from an ad hoc-designed laboratory experiment at University of Basilicata (Italy), proved that the model itself was able to grasp the global features of the phenomenon. Specifically, it mildly underestimated the field time to cutoff in pre-cutoff conditions (while mildly overestimating the corresponding bank erosion rate) and slightly underestimated the field time elapsed from cutoff in post-cutoff conditions (while slightly overestimating the corresponding bank erosion rate). In both conditions the orders of magnitude were correctly identified. It may be argued that the mismatch in estimating field times to and from cutoff could be related to variable real flow rates. Note that the mismatch (relatively slight model underestimation) refers to time intervals of about 10 years in both cases (from 1970 to 1980 and from 1980 to 1989, respectively). It is highly probable that, due to the seasonal alternation of wet and dry periods, there was a natural compensation between accelerations and decelerations of the bank erosive process related to unsteady flow conditions. We believe that the reason of a systematic bias may rather reside in the peculiar nature of meander time evolution (gradual transition from advective to purely erosional regime) whose mathematical interpretation, as later specified, constitutes the main target of the ongoing model generalization. As a matter of fact, the early stages of meander life are dominated by a strongly directional side erosion that makes it to rapidly migrate downstream, with a limited increase in amplitude. As the bend becomes longer and progressively more curved, the consequent loss of flow energy makes the bank erosion/deposition process more and more isotropic through the loop. In these conditions, its barycenter practically stops while its amplitude rapidly and highly non-linearly increases toward cutoff, in a sort of self-feeding process that relegates the effect of a hypothetical flow rate variation to a marginal role. These large-time conditions are exactly those that the present version of the model intends to reproduce by assuming the dominant role of cylinder rotation as compared to the magnitude of the external uniform flow. Indeed, by the potential flow analog expressed by Equations 7–12, which makes the intensity of the transverse bed-load (and, therefore, the intensity of the erosion/deposition phenomena) dependent on the highly nonlinearly increasing circulation Γ, our model is in principle able to account for the self-feeding meander final growth process. In the case of the laboratory experiment (which was conducted at constant flow rate), while the analytical solution closely follows neck time reduction before the breaching, the very final observations are compatible with a faster, sudden and perhaps hardly mathematically predictable collapse of the thin sandy wall. Overall, we can conclude that the proposed theoretical model seems to have the potentialities to represent a fast and easy tool to forecast the evolution of a river bend when the signs of the incipient instability suggest quantifying the time left to its exploitation (as a naturalistic or an economical resource), and to timely plan, where needed, site management and restoration. Input parameters for the application of the model to any real-life case are represented by

Table 4
River Bollin 1989 Post-Cutoff Observed and Calculated Variables

Post-cutoff 1989	
L_n (real) Hooke (1995)	67 m
r_0 (expected)	36.92 m
l_n (expected)	1.81
Γ*(from Equation B3)	5.346
τ (from Equation A19)	0.20027
$\Delta\tau_{fc}$ (theoretical)	0.05052
σ (real) Hooke (1995)	2.49
v_0/B Crosato (2009)	0.028
B (real) Hooke (1995)	9.65 m
v_0 (real)	$8.57 \cdot 10^{-9}$ m/s
Δt_{fc} (theoretical)	**7 years**
Δt_{fc} (real) Hooke (1995)	**9 years**
v_E/v_0 (from Equation B10 at $\tau = 0.20027$)	9.49
v_E (theoretical)	**2.56 m/year**
v_E (real) Hooke (1995)	**2.11 m/year**

Note. Bold values highlight the comparison between predictions and observations.

section width B, radius of the equivalent circle r_0, centerline flow depth h_0, outer bank equivalent radius and depth r_{out} and h_{out}, section-averaged velocity U and reach sinuosity σ.

5.1. Specific Limitations

1. In its present version, the model is a local one. That is, it cannot predict meanders evolution at the scale of the whole river (unless the bends do not succeed one another at a very low spatial frequency). On the other hand, in terms of practical applications, one is interested in predicting the evolution of a specific river bend in markedly instable conditions to quantify its residual regular life, and to timely and safely plan its restoration;
2. The model does not encompass geomorphological and anthropic forcing (for instance, the presence of mountain slopes or engineering works). Nevertheless, it proved to be able to correctly grasp the order of magnitude of the characteristic times from and to cutoff at a Bollin UK site, where the dying meander was clearly "compressed" and made double-headed by highly probable geological/anthropic constraints;
3. The model accounts for grain size distribution in average terms by assuming a uniform internal friction coefficient that is characteristic of sand/medium gravel (for which river meandering is indeed the most probable scenario). Nevertheless, it was able to closely simulate reality both in the lab (where, as Figures 11 and Figure 12 clearly show, bend water flow gradually induced a clear separation between fine-sediment side bars with superposed dunes and coarser active bottom, thus revealing a non-negligible sediment size heterogeneity) and on field (where sediment sorting has not even to be questioned). It should also be stressed that bars and dunes, which are always affected by non-negligible random features, considerably complicate flow field structure (e.g., Pannone, 2012; Pannone et al., 2013). When associated with the already complex 2- or 3-D realistic numerical modeling of water flow and sediment transport through a sequence of more or less pronounced bends, that may make resorting to an analytical 1-D model (which exclusively focuses on river axis evolution) a useful alternative, at least in terms of prediction of cutoff characteristic times.
4. Finally, the model does not account for the presence of vegetation, which in principle may slow down bank erosion (as a higher order effect if compared with secondary currents side action). However, it proved to be a rather robust characteristic time estimator also in this regard, when applied to vegetation-covered field banks. As a matter of fact, the progressive sedimentation of grains at the convex bank in the form of a point bar is often associated with the growth and development of vegetation that control bank dynamics. The rate of erosion of the outer bank is also influenced by riparian vegetation. Vegetation and plant root system can stabilize the bank and limit the intensity of the erosive phenomena and their timing. The authors chose, for the sake of safety, to disregard the effect of vegetation because they focused their analysis on the worst conditions, in which the reduction of outer bank erosion due to the vegetation was neglected. In this case, the highest erosion rate is expected and, everything else being the same, predicted cutoff times are shorter.

5.2. Future Research Perspectives

There is no doubt that the above-listed approximations may marginally be responsible for the non-perfect matching between theoretical predictions and real data. On the other hand, an analytical model cannot rigorously encompass the unavoidable complexity of a real process. Nevertheless, the scope of the present study was to find

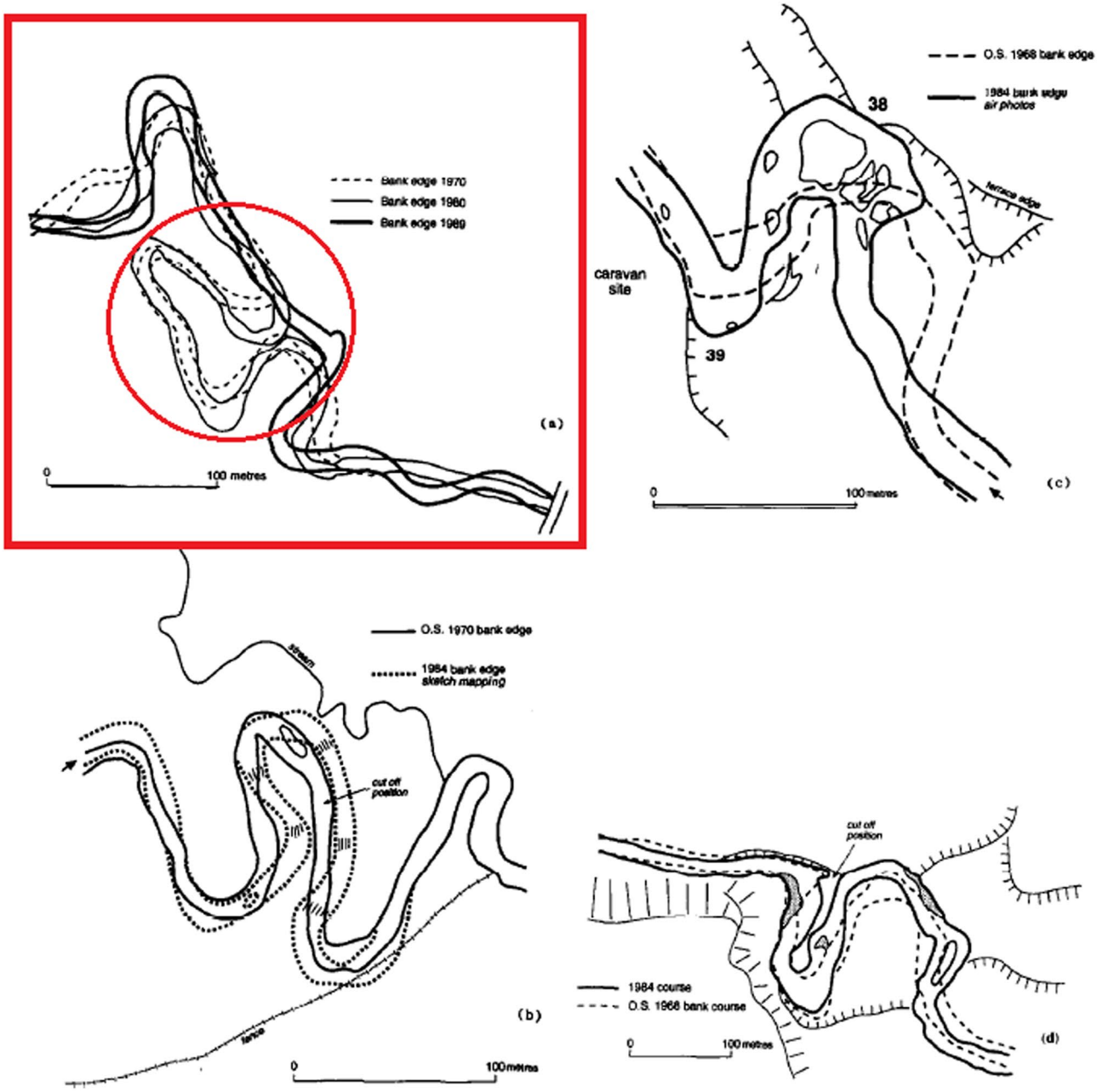

Figure 15. Bollin's cutoff site over time (see the square window and, in detail, 1980 cutoff site in the circle) (adapted from Hooke (1995) with permission). Dashed line: 1970 bank edge; full line: 1980 bank edge; thick full line: 1989 bank edge.

a fast, easy and universal prediction tool that guarantees at the same time a satisfactory predictive ability by resorting to a fully analytical formulation. With this in mind, we will further go into detail with our investigation by:

1. Verifying the possibility to calibrate the model by performing additional laboratory tests with simulated vegetation/physical constraints and even more heterogeneous gran size distributions, in order to assess the effects of suspended load involving the finer sediment fractions (e.g., Mahato et al., 2021) as well as the role of possible sedimentary singularities in determining cutoff location and direction;
2. Generalizing the theoretical model to earlier phases of meander life (farer-from-cutoff conditions) by releasing some approximations like high cylinder rotation speed/high meander axis curvature and low Reynolds number cylinder flow/low meander migration rate. We believe that this generalization can lead to the most considerable model predictive ability improvement.

Appendix A: On the Consistency of the Potential Approach in the Modeling of Near Field Velocity Around a Fast Rotating Cylinder in a Low Reynolds Number Uniform Flow

Let us start from Lamb-Oseen's linearized dimensional flow equations (Batchelor, 1967; Lamb, 1932; Oseen, 1910), with the modified boundary condition represented by cylinder rotation at constant clockwise angular rate $\Gamma/2\pi {r_0}^2$:

$$\rho\left(\boldsymbol{g}-\frac{\partial \boldsymbol{v}}{\partial t}-\boldsymbol{v}_0''\cdot\nabla\boldsymbol{v}\right)=\nabla p-\mu\nabla^2\boldsymbol{v} \tag{A1}$$

$$\nabla\cdot\boldsymbol{v}=0 \tag{A2}$$

$$v_c=\|\boldsymbol{v}\|_c=-\frac{\Gamma}{2\pi r_0} \tag{A3}$$

where $\boldsymbol{v}$ indicates the generic velocity vector, $\boldsymbol{v}_0''=v_0''\hat{\boldsymbol{x}}$ the velocity of the incompressible flow that hits the cylinder (or, equivalently, the velocity at which the cylinder moves through the static fluid along the opposite longitudinal direction), $\boldsymbol{g}=-g\hat{\boldsymbol{z}}$ the gravity acceleration vector, z the vertical coordinate, subscript c the cylinder contour, and the double vertical brackets the vector magnitude. Total velocity may then be subdivided into a potential ($\boldsymbol{v}_0''+\boldsymbol{v}_1$) and a deviatory rotational ($\boldsymbol{v}_2$) component (Marchi & Rubatta, 1981). For steady flow, let:

$$-\nabla(\gamma z+p)+\mu\nabla^2\boldsymbol{v}=\rho v_0''\frac{\partial \boldsymbol{v}}{\partial x} \tag{A4}$$

with $\gamma=\rho g$ indicating fluid specific weight. The $\boldsymbol{v}_2$-related conditions for the proposed flow field $\boldsymbol{v}=\boldsymbol{v}_0''+\boldsymbol{v}_1+\boldsymbol{v}_2$ being a possible solution of Equations A1 and A2 are continuity and residual momentum, that is:

$$\nabla\cdot\boldsymbol{v}_2=0 \tag{A5}$$

and

$$\nabla^2\boldsymbol{v}_2-\frac{v_0''}{\nu}\frac{\partial \boldsymbol{v}_2}{\partial x}=0 \tag{A6}$$

where $\nu=\mu/\rho$ indicates kinematic viscosity. Series solution of Equation A6 for small $v_0''r/2\nu$ yields (e.g., Batchelor, 1967; Marchi & Rubatta, 1981):

$$v_{2x}=c_0\left[\frac{1}{2}\left(E_u-\frac{1}{2}+\ln\frac{v_0''r}{4\nu}\right)-\frac{\nu}{v_0''}\frac{\partial \ln r}{\partial x}+\frac{1}{4}r^2\frac{\partial^2\ln r}{\partial x^2}+\ldots\right] \tag{A7}$$

$$v_{2y}=c_0\left[-\frac{\nu}{v_0''}\frac{\partial \ln r}{\partial y}+\frac{1}{4}r^2\frac{\partial^2\ln r}{\partial x\partial y}+\ldots\right] \tag{A8}$$

with $r=\sqrt{x^2+y^2}$ and E_u indicating Euler's constant. The mathematical shape of Equations A7 and A8, and the boundary condition (30) $\|\boldsymbol{v}\|_c\equiv v_\theta(r_0,\theta)=-\Gamma/2\pi r_0$, where $\theta=\tan^{-1}(y/x)$, suggest assuming the following potential function for the irrotational component of the flow:

$$\varphi=v_0''x-\frac{\Gamma}{2\pi}\tan^{-1}\left(\frac{y}{x}\right)+c_1\ln r+c_2\frac{\partial \ln r}{\partial x}+\ldots \tag{A9}$$

with:

$$\frac{\partial\varphi}{\partial x}=v_0''+v_{1x} \tag{A10}$$

$$\frac{\partial\varphi}{\partial y}=v_{1y} \tag{A11}$$

and the constants respectively given by:

$$c_0 = \frac{2v_0''}{\left(\frac{1}{2} - E_u - \ln\frac{v_0'' r_0}{4\nu}\right)} \tag{A12}$$

$$c_1 = \frac{\nu}{v_0''} c_0 \tag{A13}$$

$$c_2 = -\frac{r_0^2}{4} c_0 \tag{A14}$$

Total Cartesian components of velocity will therefore be expressed as:

$$v_x = v_0'' + v_{1x} + v_{2x} = v_0' \ln\frac{r}{r_0} + v_0' \left(1 - \frac{r_0^2}{r^2}\right) \frac{\left(1 - 2\cos^2\theta\right)}{2} + \frac{\Gamma}{2\pi r}\sin\theta \tag{A15}$$

$$v_y = v_{1y} + v_{2y} = -v_0' \left(1 - \frac{r_0^2}{r^2}\right) \sin\theta\cos\theta - \frac{\Gamma}{2\pi r}\cos\theta \tag{A16}$$

where

$$v_0' = \frac{v_0''}{\left(\frac{1}{2} - E_u - \ln\frac{v_0'' r_0}{4\nu}\right)} = \frac{v_0''}{\left(\frac{1}{2} - E_u - \ln\frac{Re}{8}\right)} \tag{A17}$$

or, in the cylindrical reference frame:

$$v_r = v_x\cos\theta + v_y\sin\theta = v_0' \ln\frac{r}{r_0}\cos\theta - \frac{v_0'}{2}\left(1 - \frac{r_0^2}{r^2}\right)\cos\theta = \frac{1}{r}\frac{\partial\Psi}{\partial\theta} \tag{A18}$$

$$v_\theta = -v_x\sin\theta + v_y\cos\theta = -v_0' \ln\frac{r}{r_0}\sin\theta - \frac{v_0'}{2}\left(1 - \frac{r_0^2}{r^2}\right)\sin\theta - \frac{\Gamma}{2\pi r} = -\frac{\partial\Psi}{\partial r} \tag{A19}$$

where Ψ indicates the associated stream function. The solution of the above partial differential equation system leads to:

$$\Psi(r,\theta) = -\frac{v_0'}{2}\left(r - \frac{r_0^2}{r}\right)\sin\theta + v_0' r \ln\frac{r}{r_0}\sin\theta + \frac{\Gamma}{2\pi}\ln r \tag{A20}$$

or:

$$\Psi(r,\theta) = -\frac{v_0'}{2}\left(r - \frac{r_0^2}{r}\right)\sin\theta + \frac{\Gamma}{2\pi}\left(\frac{2\pi v_0' r}{\Gamma}\ln\frac{r}{r_0}\sin\theta + \ln r\right) \tag{A21}$$

At relatively high rotation speeds, with $-v_0' = 2v_0$, $\Gamma \gg 4\pi v_0 r_0$, and finite r/r_0:

$$\Psi(r,\theta) = v_0\left(r - \frac{r_0^2}{r}\right)\sin\theta + \frac{\Gamma}{2\pi}\left(-\frac{4\pi v_0 r_0}{\Gamma}\frac{r}{r_0}\ln\frac{r}{r_0}\sin\theta + \ln r\right) \cong v_0\left(r - \frac{r_0^2}{r}\right) + \frac{\Gamma}{2\pi}\ln r \tag{A22}$$

which indeed represents the stream-function of a potential flow field made by a longitudinal uniform flow of velocity v_0 superposed to a doublet of constant $m = 2\pi v_0 {r_0}^2$ and a clockwise free vortex of circulation Γ, the last two centered at the origin of the reference frame (e.g., Batchelor, 1967; Marchi & Rubatta, 1981). Note that the condition $\Gamma \gg 4\pi v_0 r_0$ is equivalent to:

$$\ln\frac{Re}{8} \ll \frac{1}{2} - E_u - \frac{2\pi r_0 v_0''}{\Gamma} \tag{A23}$$

Equation A23 consistently means that, the larger the circulation, the larger the Reynolds number that guarantees the reliability of the truly potential-flow formulation, according to Padrino and Joseph's (2006) numerical findings.

Appendix B: Circulation/Meander Amplitude Analytical Solution

Being understood that, according to Equation A23, at small rotation speeds (the equivalent of early meander instability) the present formulation may be considered as an approximation that is as closer to reality as slower the uniform flow/meander migration is, for $\Gamma^* \to 0^+$ we obtain from Equations 15–17:

$$\begin{aligned}\frac{d\Gamma^*}{d\tau} &\cong \frac{2\Gamma^{*2}\tan\alpha}{\sqrt{2}\pi^2\Gamma^{*3/2}}\int_0^\pi |-\Gamma^* - 8\pi\sin\theta|^{3/2}d\theta = \\ &= \frac{2}{\sqrt{2}\pi^2}\tan\alpha\Gamma^{*1/2}\int_0^\pi (\Gamma^* + 8\pi\sin\theta)^{3/2}d\theta\end{aligned} \tag{B1}$$

Series expansion of the integrand in Equation B1 leads to:

$$\frac{d\Gamma^*}{d\tau} \cong \frac{2(8\pi)^{3/2}}{\sqrt{2}\pi^2}\tan\alpha\Gamma^{*1/2}\int_0^\pi \sin^{3/2}\theta\left(1+\frac{3\Gamma^*}{16\pi\sin\theta}\right)d\theta \tag{B2}$$

and, after performing the angular integration:

$$\frac{d\Gamma^*}{d\tau} = k_1\Gamma^{*1/2} + k_2\Gamma^{*3/2} \tag{B3}$$

with

$$k_1 = 64\sqrt{\frac{2}{\pi}}\frac{G^2\left(\frac{5}{4}\right)}{G\left(\frac{5}{2}\right)}\tan\alpha \tag{B4}$$

$$k_2 = \frac{12}{\pi\sqrt{2\pi}}\frac{G^2\left(\frac{3}{4}\right)}{G\left(\frac{3}{2}\right)}\tan\alpha \tag{B5}$$

and G indicating Gamma Function. Finally, the integration of the ordinary differential Equation B3 yields (Gradshteyn & Ryzhik, 1994):

$$\Gamma_1^*(\tau) = \frac{k_1}{k_2}\tan^2\left(\frac{k_1}{2}\sqrt{\frac{k_2}{k_1}}\tau\right) \tag{B6}$$

For large Γ^* ($\Gamma^* >> 4\pi$) and from the potential flow theory, the y-coordinate of the single, off-cylinder stagnation point ($x_s = 0$) is:

$$y_s = \frac{\Gamma}{4\pi v_0} + \frac{r_0}{4\pi}\sqrt{\frac{\Gamma^2}{v_0^2 r_0^2} - 16\pi^2} \cong \frac{\Gamma}{2\pi v_0} \tag{B7}$$

and, in differential terms:

$$dy_S = \frac{d\Gamma}{2\pi v_0} \tag{B8}$$

with the fluid-dynamic power given by:

$$P = \frac{\rho\Gamma}{2\pi}\frac{d\Gamma}{dt} \tag{B9}$$

Therefore, for the closed loop (with the angular coordinate that goes from 0 to 2π):

$$\frac{d\Gamma^*}{d\tau} = \frac{\Gamma^{*2}}{\sqrt{2}\pi^2}\tan\alpha\int_0^{2\pi}\left|-1-\frac{8\pi\sin\theta}{\Gamma^*}\right|^{3/2}d\theta = \\ = \frac{\Gamma^{*2}}{\sqrt{2}\pi^2}\tan\alpha\int_0^{2\pi}\left(1+\frac{8\pi\sin\theta}{\Gamma^*}\right)^{3/2}d\theta \tag{B10}$$

Series expansion of the integrand in Equation B10 for $\Gamma^* \to \infty$ leads to:

$$\frac{d\Gamma^*}{d\tau} \cong \frac{\Gamma^{*2}\tan\alpha}{\sqrt{2}\pi^2}\int_0^{2\pi}\left(1+\frac{12\pi}{\Gamma^*}\sin^2\theta+\frac{24\pi^2}{\Gamma^{*2}}\sin^2\theta\right)d\theta = \\ = \frac{1}{\sqrt{2}\pi^2}\tan\alpha\left(2\pi\Gamma^{*2}+24\pi^3\right) \tag{B11}$$

Finally, the integration of differential Equation B11 yields (Gradshteyn & Ryzhik, 1994):

$$\Gamma^* = \sqrt{12\pi^3}\tan(\sqrt{24\pi}\tan\alpha\tau + C) \tag{B12}$$

with C indicating a numerical constant. As above mentioned, the overlapping of the two limiting solutions at medium circulation values is obtained by imposing the matching of their respective extrapolations at $\Gamma^* = 4\pi$ (as done in Figure 5), thus obtaining $C = -0.9469$.

Conflict of Interest

The authors declare no conflicts of interest relevant to this study.

Data Availability Statement

The data used in this study were either reported elsewhere (Hooke, 1995, 2004) or were made directly available in the paper by text, figures and tables.

Acknowledgments
This research has been supported by University of Basilicata under projects L.IDRO.AM.BIO (Laboratory of environmental and biological hydrodynamics) U.P.B. Pannone17 and S.PO.T.S.A.B. (Stream power and solid transport in braided beds) U.P.B. De Vincenzo16. Open Access Funding provided by Universita degli Studi della Basilicata within the CRUI-CARE Agreement.

References

Asahi, K., Shimizu, Y., Nelson, J., & Parker, G. (2013). Numerical simulation of river meandering with self-evolving banks. *Journal of Geophysical Research: Earth Surface*, *118*(4), 2208–2229. https://doi.org/10.1002/jgrf.20150

Bagnold, R. A. (1966). *An approach to the sediment transport problem from general physics, Physiographic and hydraulic studies of rivers*. In *Geological Survey Professional Paper* (Vol. 422-I). United States Government Printing Office. https://doi.org/10.3133/pp422I

Batchelor, G. K. (1967). *An introduction to fluid dynamics* (p. 615). Cambridge University Press.

Brice, J. C. (1974). Evolution of meander loops. *Bulletin of the Geological Society of America*, *85*(4), 581–586. https://doi.org/10.1130/0016-7606(1974)85<581:EOML>2.0.CO;2

Camporeale, C., Perona, P., Porporato, A., & Ridolfi, L. (2005). On the long-term behavior of meanderig rivers. *Water Resources Research*, *41*(12), W12403. https://doi.org/10.1029/2005WR004109

Camporeale, C., Perucca, E., & Ridolfi, L. (2008). Significance of cutoff in meandering river dynamics. *Journal of Geophysical Research*, *113*(F1), F01001. https://doi.org/10.1029/2006JF000694

Carlston, C. W. (1965). The relation of free meander geometry to stream discharge and its geomorphic implications. *American Journal of Science*, *263*(10), 864–885. https://doi.org/10.2475/ajs.263.10.864

Constantine, J. A., McLean, S. R., & Dunne, T. (2010). A mechanism of chute cutoff along large meandering rivers with uniform floodplain topography. *The Geological Society of America Bulletin*, *122*(5–6), 855–869. https://doi.org/10.1130/B26560.1

Crosato, A. (2009). Physical explanations of variations in river meander migration rates from model comparison. *Earth Surface Processes and Landforms*, *34*(15), 2078–2086. https://doi.org/10.1002/esp.1898

De Vincenzo, A., Brancati, F., & Pannone, M. (2016). An experimental analysis of bed load transport in gravel-bed braided rivers with high grain Reynolds numbers. *Advances in Water Resources*, *94*, 160–173. https://doi.org/10.1016/j.advwatres.2016.05.007

Dey, S., & Ali, S. Z. (2020). Fluvial instability. *Physics of Fluids*, *33*(6), 061301. https://doi.org/10.1063/5.0010038

Einstein, H. A. (1950). *The bed load function for sediment transportation in open channel flows*. U.S. Department of Agriculture. Tech. Bull. 1026, Soil Conserv. Serv.

Eke, E., Parker, G., & Yasuyuki, S. (2014). Numerical modeling of erosional and depositional bank processes in migrating river bends with self-formed width: Morphodynamics of bar push and bank pull. *Journal of Geophysical Research*, *119*(7), 1455–1483. https://doi.org/10.1002/2013jf003020

Eke, E. C., Czapiga, M. J., Viparelli, E., Shimizu, Y., Imran, J., Sun, T., & Parker, G. (2014). Coevolution of width and sinuosity in meandering rivers. *Journal of Fluid Mechanics*, *760*, 127–174. https://doi.org/10.1017/jfm.2014.556

Ferguson, R. I. (1984). Kinematic model of meander migration. In C. M. Elliott (Ed.), *River meandering ASCE* (pp. 942–951). Am. Soc. of Civ. Eng.
Frascati, A., & Lanzoni, S. (2009). Morphodynamic regime and long-term evolution of meandering rivers. *Journal of Geophysical Research*, *114*(F2), F02002. https://doi.org/10.1029/2008JF001101
Gay, G. R., Gay, H. H., Gay, W. H., Martinson, H. A., Meade, R. H., & Moody, J. A. (1998). Evolution of cutoffs across meander necks in Powder River, Montana, USA. *Earth Surface Processes and Landforms*, *23*(7), 651–662. https://doi.org/10.1029/2006JF000694
Gradshteyn, I. S., & Ryzhik, I. M. (1994). *Table of integrals, series, and products* (5th ed.). Academic Press Inc.1204.
Grenfell, M., Aalto, R., & Nicholas, A. (2012). Chute channel dynamics in large, sand-bed meandering rivers. *Earth Surface Processes and Landforms*, *37*(3), 315–331. https://doi.org/10.1002/esp.2257
Grenfell, M., Michael, C., Nicholas, A. P., & Aalto, R. (2014). Mediative adjustment of river dynamics: The role of chute channels in tropical sand-bed meandering rivers. *Sedimentary Geology*, *301*, 93–106. https://doi.org/10.1016/j.sedgeo.2013.06.007
Han, B., & Endreny, T. A. (2014). Detailed river stage mapping and head gradient analysis during meander cutoff in a laboratory river. *Water Resources Research*, *50*(2), 1689–1703. https://doi.org/10.1002/2013WR013580
Hansen, E. (1967). *The formation of meanders as a stability problem, basic res. Prog. Rep. 13, hydraul. Lab*. Lyngby.
Hasegawa, K. (1989). Universal bank erosion coefficient for meandering rivers. *Journal of Hydraulic Engineering*, *115*(6), 744–765. https://doi.org/10.1061/(asce)0733-9429(1989)115:6(744)
Hickin, E. J., & Nanson, G. C. (1984). Lateral migration rates of river bends. *Journal of Hydraulic Engineering*, *110*(11), 1557–1567. https://doi.org/10.1061/(ASCE)0733-9429(1984)110:11(1557)
Hooke, J. M. (1995). River channel adjustment to meander cutoffs on the River Bollin and River Dane, northwest England. *Geomorphology*, *14*(3), 235–253. https://doi.org/10.1016/0169-555X(95)00110-Q
Hooke, J. M. (2004). Cutoffs galore!: Occurrence and causes of multiple cutoffs on a meandering river. *Geomorphology*, *61*(3–4), 225–238. https://doi.org/10.1016/j.geomorph.2003.12.006
Howard, A. D. (1984). Simulation model of meandering. In C. M. River Meandering (Ed.), *River meandering ASCE* (pp. 952–963). Am. Soc. of Civ. Eng.
Ikeda, S., Parker, G., & Sawai, K. (1981). Bend theory of river meanders. Part 1. Linear development. *Journal of Fluid Mechanics*, *112*(-1), 363–377. https://doi.org/10.1017/S0022112081000451
Johnson, R. H., & Paynter, J. (1967). The development of a cutoff on the river irk at chadderton, lancashire. *Geography*, *52*, 41119.
Lamb, H. (1932). *Hydrodynamics* (6th ed., pp. 614–617). Cambridge University Press.
Lancaster, S. T., & Bras, R. L. (2002). A simple model of river meandering and its comparison to natural channels. *Hydrological Processes*, *16*, 1–26. https://doi.org/10.1002/hyp.273
Leopold, L. B., & Wolman, M. G. (1960). River meanders. *The Geological Society of America Bulletin*, *71*(6), 769–794. https://doi.org/10.1130/0016-7606(1960)71[769:rm]2.0.co;2
Lewis, G. W., & Lewin, J. (1983). Alluvial cutoffs in wales and the borderlands. In J. D. Collinson & J. Lewin (Eds.), *Modern and ancient fluvial systems* (pp. 145–154). Blackwell Publishing Ltd. https://doi.org/10.1002/9781444303773.ch11
Li, Z., Gao, P., & Wu, X. (2022). Processes of neck cutoff and channel adjustment affected by seeding herbaceous vegetation and variable discharges. *Catena*, *208*, 105731. https://doi.org/10.1016/j.catena.2021.105731
Mahato, R. K., Dey, S., & Ali, S. Z. (2021). Instability of a meandering channel with variable width and curvature: Role of sediment suspension. *Physics of Fluids*, *33*(11), 111401. https://doi.org/10.1063/5.0074974
Mahato, R. K., Dey, S., & Ali, S. Z. (2022). Planform evolution of a sinuous channel triggered by curvature and autogenic width oscillations due to generic grain transport. *Physics of Fluids*, *34*(4), 044110. https://doi.org/10.1063/5.0087971
Marchi, E., & Rubatta, A. (1981). *Meccanica dei Fluidi – principi ed applicazioni idrauliche* (p. 800). UTET.
Meyer-Peter, E., & Müller, R. (1948). Formulas for bed load transport. In *Proceedings of 2nd meeting of international association for hydraulic structures research* (pp. 39–64).
Mosley, M. P. (1975). Meander cutoffs on the river Bollin, cheshire. *Revue de Geomorphologie Dynamique*, *24*, 21–32.
Odgaard, A. J. (1984). *Bank erosion contribution to stream sediment load*, Iowa Institute of Hydraulic Research Report No. 280, The University of Iowa.
Odgaard, A. J. (1987). Streambank erosion along two rivers in Iowa. *Water Resources Research*, *23*(7), 1225–1236. https://doi.org/10.1029/WR023i007p01225
Oseen, C. W. (1910). Uber die Stokessche Formel und uber eine verwandte Aufgabe in der Hydrodynamik. *Arkiv för matematik, astronomi och fysik*, *6*(29).
Padrino, J. C., & Joseph, D. D. (2006). Numerical study of the steady-state uniform flow past a rotating cylinder. *Journal of Fluid Mechanics*, *557*, 191–223. https://doi.org/10.1017/S0022112006009682
Pannone, M. (2012). Longitudinal dispersion in river flows characterized by random large-scale bed irregularities: First order analytical solution. *Journal of Hydraulic Engineering*, *138*(5), 400–411. https://doi.org/10.1061/(ASCE)HY.1943-7900.0000537
Pannone, M., & De Vincenzo, A. (2021). Theoretical investigation of equilibrium dynamics in braided gravel beds for the preservation of a sustainable fluvial environment. *Sustainability*, *13*(3), 1246. https://doi.org/10.3390/su13031246
Pannone, M., De Vincenzo, A., & Brancati, F. (2013). A mathematical model for the flow resistance and the related hydrodynamic dispersion induced by river dunes. *Journal of Applied Mathematics*, *2013*(9), 432610. https://doi.org/10.1155/2013/432610
Parker, G. (1976). On the cause and characteristic scales of meandering and braiding in rivers. *Journal of Fluid Mechanics*, *76*(3), 457–480. https://doi.org/10.1017/S0022112076000748
Parker, G., Shimizu, Y., Wilkerson, G. V., Eke, E. C., Abad, J. D., Lauer, J. W., et al. (2011). A new framework for modeling the migration of meandering rivers. *Earth Surface Processes and Landforms*, *36*(1), 70–86. https://doi.org/10.1002/esp.2113
Peakall, J., Ashworth, P., & Best, J. (1996). Physical modeling in fluvial geomorphology: Principles, applications and unresolved issues. In *The scientific nature of geomorphology, proceedings of the 27th binghamton symposium of geomorphology* (pp. 221–253).
Richard, G. A., Julien, P. Y., & Baird, D. C. (2005). Statistical analysis of lateral migration of the Rio Grande, New Mexico. *Geomorphology*, *71*(1–2), 139–155. https://doi.org/10.1016/j.geomorph.2004.07.013
Richards, D., & Konsoer, K. (2019). Morphologic adjustments of actively evolving highly curved neck cutoffs. *Earth Surface Processes and Landforms*, *45*(4), 1067–1081. https://doi.org/10.1002/esp.4763
Seminara, G., Zolezzi, G., Tubino, M., & Zardi, D. (2001). Downstream and upstream influence in river meandering. Part 2. Planimetric development. *Journal of Fluid Mechanics*, *438*, 213–230. https://doi.org/10.1017/S0022112001004281
Smith, J. D., & McLean, S. R. (1984). A model for flow in meandering streams. *Water Resources Research*, *20*(9), 1301–1315. https://doi.org/10.1029/WR020i009p01301

Stølum, H. H. (1996). River meandering as a self-organization process. *Science*, *271*(5256), 1710–1713. https://doi.org/10.1126/science.271.5256.1710

Sun, T., Meakin, P., Jossang, T., & Schwarz, K. (1996). A simulation model for meandering rivers. *Water Resources Research*, *32*(9), 2937–2954. https://doi.org/10.1029/96WR00998

Van Dijk, W. M., Schuurman, F., Van de Lageweg, W. I., & Kleinhans, M. G. (2014). Bifurcation instability determines chute cutoff development in meandering gravel-bed rivers. *Geomorphology*, *213*, 277–291. https://doi.org/10.1016/j.geomorph.2014.01.018

Van Dijk, W. M., Van de Lageweg, W. I., & Kleinhans, M. G. (2012). Experimental meandering river with chute cutoffs. *Journal of Geophysical Research*, *117*(F3), F03023. https://doi.org/10.1029/2011/JF002314

Wallick, J. R., Lancaster, S. T., & Bolte, J. P. (2006). Determination of bank erodibility for natural and anthropogenic bank materials using a model of lateral migration and observed erosion along the Willamette River, Oregon, USA. *River Research and Applications*, *22*(6), 631–649. https://doi.org/10.1002/rra.925

Yalin, M. S. (1992). *River mechanics* (p. 219). Pergamon Press Ltd, Headington Hill Hall.

Yilmaz, L. (2008). Experimental study of sediment transport in meandering channels. *Water Resources Management*, *22*(2), 259–275. https://doi.org/10.1007/s11269-007-9156-1

Zen, S., Zolezzi, G., Toffolon, M., & Gurnell, A. M. (2016). Biomorphodynamic modelling of inner bank advance in migrating meander bends. *Advances in Water Resources*, *93*, 166–181. https://doi.org/10.1016/j.advwatres.2015.11.017

Zinger, J. A., Rhoads, B. L., & Best, J. L. (2011). Extreme sediment pulses generated by bend cutoffs along a large meandering river. *Nature Geoscience*, *4*(10), 675–678. https://doi.org/10.1038/ngeo1260

Zinger, J. A., Rhoads, B. L., Best, J. L., & Johnson, K. K. (2013). Flow structure and channel morphodynamics of meander bend chute cutoffs: A case study of the wabash river, USA. *Journal of Geophysical Research: Earth Surface*, *118*(4), 2468–2487. https://doi.org/10.1002/jgrf.20155

Zolezzi, G., & Seminara, G. (2001). Downstream and upstream influence in river meandering. Part 1. General theory and application to overdeepening. *Journal of Fluid Mechanics*, *438*, 183–211. https://doi.org/10.1017/s002211200100427x